Research Square

Preprints are preliminary reports that have not undergone peer review.
They should not be considered conclusive, used to inform clinical practice,
or referenced by the media as validated information.

Design and Simulation of a Fully Automated Fresh-Packaging Integrated Machine for Pakchoi

Lin Zongde

524609658@qq.com

Minnan University of Science and Technology

Yu Ping

Minnan University of Science and Technology

Lin Peng

Minnan University of Science and Technology

Deng Jiakun

Minnan University of Science and Technology

Xue Hongwei

Minnan University of Science and Technology

Lai Shengwei

Minnan University of Science and Technology

Huang Senhui

Minnan University of Science and Technology

Article

Keywords: pakchoi processing machine, structural design, finite element analysis, automation, integrated packaging

Posted Date: March 30th, 2026

DOI: https://doi.org/10.21203/rs.3.rs-9148654/v1

License: This work is licensed under a Creative Commons Attribution 4.0 International License.
Read Full License

Additional Declarations: No competing interests reported.

Design and Simulation of a Fully Automated Fresh-Packaging Integrated Machine for Pakchoi

Lin Zongde[1*], Yu Ping[1], Lin Peng[1], Deng Jiakun[1], Xue Hongwei[1], Lai Shengwei[1], Huang Senhui[1]

1 Minnan University of Science and Technology，Shishi 362700; 524609658@qq.com

* Minnan University of Science and Technology，Shishi 362700; Correspondence: 524609658@qq.com; Tel.: 15860536885

Abstract

In response to the growing demand for automated and standardized post-harvest processing of leafy pakchois, this study addresses the existing bottleneck in which current equipment fails to accommodate the fragile and perishable nature of leaf pakchois and lacks integrated solutions. A fully automatic, fresh-processing, and packaging integrated machine for pakchoi has been designed and developed. The system incorporates a modular architecture that integrates root removal, yellow-leaf elimination, washing, and packaging functions. The structural reliability of key components was verified through finite element simulation, with safety factors exceeding 8. Multi-process coordination and sequential control were implemented using an STM32-based controller. Performance tests demonstrated a processing capacity of ⩾50 kg/h, along with 100% root-removal rate, ⩾98% yellow-leaf removal rate, and ⩽3% damage rate. This research provides a feasible technical pathway for low-loss, efficient, and standardized post-harvest handling of leafy pakchois, offering practical implications for promoting pakchoi commercialization and industrial automation.

Keywords: pakchoi processing machine; structural design; finite element analysis; automation; integrated packaging

1. Introduction

With the increasing awareness of food safety and the ongoing consumption upgrading among urban and rural residents, the demand for clean and standardized packaging of leafy pakchois such as pakchoi continues to grow (Luan et al., 2021). Currently, however, the post-harvest processing of pakchoi remains predominantly reliant on manual labor, characterized by low efficiency (typically only 20–30 kg per hour per worker), inconsistent cleaning outcomes, and labor costs constituting over 35% of the total operational expenses (EFSA Panel on Biological Hazards (BIOHAZ) et al., 2023). These challenges significantly constrain the industry's progress toward scale and standardized development ('Accelerating the Pilot Verification and Maturation Application of Innovative Agricultural Machinery Products', 2025). Moreover, existing fruit and pakchoi processing equipment is mostly designed for root crops or fruit, rendering it unsuitable for the tender and easily damaged nature of leafy greens (Shi et al., 2021). In particular, integrated automated solutions that combine root removal, yellow leaf removal, and packaging are notably lacking.

Internationally, automation technologies for post-harvest processing of leafy pakchois have made significant advances, such as the use of near-infrared spectroscopy and machine vision

for quality sorting (Da Silva et al., 2020), and the application of flexible actuators to reduce mechanical damage (Martinez et al., 2014). Nevertheless, most existing research focuses on single processing stages or high-value horticultural crops. Studies and industrial implementations of low-cost, fully integrated processing equipment aimed at high-volume leafy pakchois like pakchoi remain relatively scarce. In China, relevant research has paid closer attention to alignment with local production practices, with valuable explorations carried out in areas such as hydrodynamic optimization for pakchoi cleaning (Palamarchuk et al., 2021) and control system design based on commonly used PLCs (Estévez et al., 2007). That said, gaps still exist compared to international advanced levels in the integration of high-end sensors and mechatronic systems, and the translation of related technological achievements into small- to medium-scale production equipment remains relatively slow.

In this context, developing a fully automated processing system that integrates root removal, yellow leaf removal, washing, 90° orientation adjustment, and packaging functions would address multiple shortcomings of manual handling, substantially enhance the commercial quality of leafy pakchois, effectively reduce operational costs, and carry important practical significance for advancing agricultural mechanization and ensuring food safety.

2. Functional Analysis

Based on the processing requirements and market demand for pakchoi, this design follows the principles of automation, high efficiency, and low damage. Pakchoi has a tender texture, with thin leaves and high water content. The overall plant length typically ranges from 200 mm to 300 mm, and the root-end diameter generally does not exceed 250 mm. The petioles (stems) exhibit relatively low fiber strength and small cross-sectional dimensions (approximately 3–5 mm) (Henny & Gobilik, n.d.), making them prone to crushing, tearing, or breaking under mechanical action. Moreover, their irregular shape, loose leaf arrangement, and large projected area pose challenges for mechanized grasping, positioning, and arranging. Considering these material characteristics, the core functions of the equipment are defined as follows:

(1)Fully automated whole-process operation: Implements seven consecutive steps—feeding, root excision, yellow-leaf removal, washing, 90° orientation change, air-drying, and tying-packaging—in a fully automated pipeline without manual intervention.

(2)Precise separation performance: Integrates mechanical compression with rotary cutting for accurate root cutting. Machine-vision recognition (Zhang Minggui et al., 2024), combined with flexible gripping technology, enables nondestructive removal of yellow leaves, achieving high separation accuracy and low damage rate.

(3)High-efficiency cleaning: Adopts a roller-conveyor and spray-nozzle system to ensure all-around rinsing of leaves. The design meets the required sediment-removal rate while maintaining reasonable water consumption.

(4)Regularized quantitative packaging: A worm-and-worm-wheel transmission rotates the pakchoi by 90° and delivers it to the downstream station. A rotating ring-wheel wrapping mechanism performs standardized bundling, with packaging weight error kept within the acceptable range.

(5)Intelligent control: The control system is built around an STM32 microcontroller and is equipped with a visual human-machine interface. It supports multi-process sequence coordination, real-time status monitoring, fault pre-warning, and user-friendly interaction.

3. Equipment Structural Design

This chapter details the structural design of the machine, which adopts a zigzag layout and a modular integration strategy. The design is elaborated in the following six aspects: the purification module, the quantitative packaging module, the conveying mechanism, the overall dimensioning, the material selection, and the control system. To realize the intended functions efficiently, the equipment is spatially optimized with a zigzag configuration, integrating two core modules—purification treatment and quantitative packaging. The main structural designs are as follows:

3.1. Purification Treatment Module

This section presents the mechanical design of the purification treatment module, which mainly consists of three core functional mechanisms: root removal, yellow-leaf removal, and washing.

3.1.1. Root-Removal Mechanism

The mechanism adopts a torsion-spring-based compression design, consisting of a baffle plate, a pressing plate, torsion springs, rotating blades, and a conveyor belt. After the pakchoi is positioned, the pressing plate compresses the pakchoi body under the action of the springs (Liu Shihao et al., 2017). Simultaneously, rotating blades (300 r/min) cut off the roots. The drive motor has a rated torque of 15 N·m, ensuring a neat cut. A schematic of the mechanism is shown in Fig. 1.

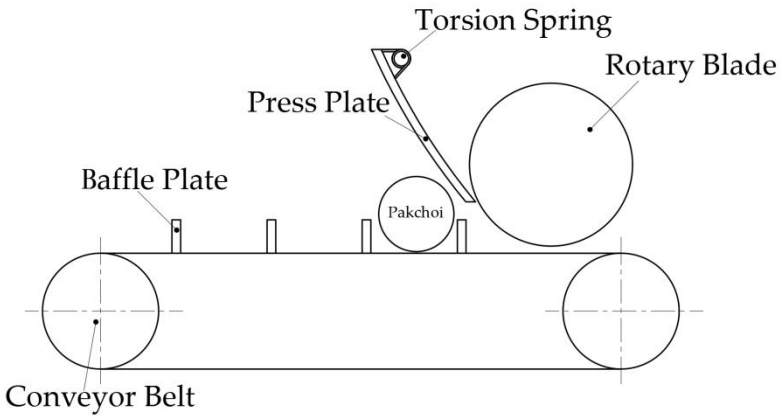


Fig. 1. Schematic of the root-removal mechanism.

The drive motor rotates the blade shaft through a chain transmission. To assess the structural safety, the strength of the critical blade-connecting shaft must be verified. The shaft is made of 45 steel, with an input power P=2.5 kW and a rotational speed n= 300 r/min. The bending moment obtained via the cross-section method is M=15 000 N·mm. The safety factor of the shaft, Sca, is given by the formula：

$$\begin{cases} S_\sigma = \dfrac{\sigma_{-1}}{K_\sigma \sigma + \varphi_\sigma \sigma_m} \\ S_\tau = \dfrac{\sigma_{-1}}{K_\tau \tau + \varphi_\tau \tau_m} \\ S_{ca} = \dfrac{S_\sigma S_\tau}{\sqrt{S_\sigma^2 + S_\tau^2}} \end{cases} \quad (1)$$

where Sσ and Sτ are the bending- stress and shear-stress safety factors, Kσ and Kτ are the corresponding fatigue-limit composite coefficients, σ and τ are the bending and shear stresses, MPa; and σm and τm are the compressive stress and compressive shear stress induced by the axial force, MPa. The calculated safety factor is 5.52, which meets the design requirement.

3.1.2. Yellow-Leaf-Removal Mechanism

The core components include a cross slide, a flexible gripper, rollers, a leaf-pushing rod, a pressing plate, and a vision sensor. The vision sensor is mounted at the tip of the flexible gripper (DONG Tingjian et al., 2023) for leaf-feature recognition. The cross slide is connected to the frame through linear guides, providing X/Y-axis motion for the gripper (Hao & Hand, 2016). Two sets of support rollers, arranged symmetrically at the base, rotate the pakchoi. The pressing plate is installed above the rollers, while the leaf-pushing rod is positioned horizontally on the side. These components respectively realize clamping of the pakchoi and material transfer between processes (Yang et al., 2025). A schematic of the mechanism is shown in Fig. 2.

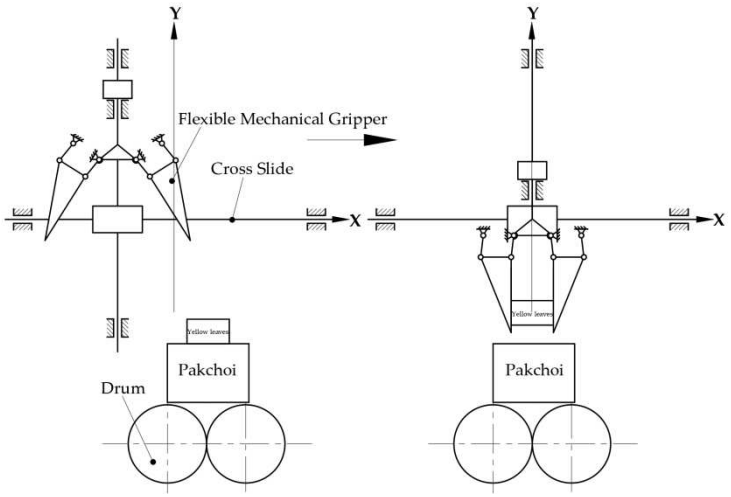


Fig. 2. Schematic of the yellow-leaf removal mechanism.

3.1.3. Washing Mechanism

This unit consists of a roller-conveyor assembly, a spray system, and a water tank. Nine rollers made of Q235 steel (diameter 50 mm, length 300 mm) tumble the pakchoi continuously (HE Xiaodong et al., 2020), while multiple high-pressure spray nozzles provide all-round rinsing to ensure complete cleaning without dead zones. The resulting wastewater is collected centrally and treated in the system (Zhao Yongcheng & Luo Jinhai, 2025). A schematic of the mechanism is shown in Fig. 3.

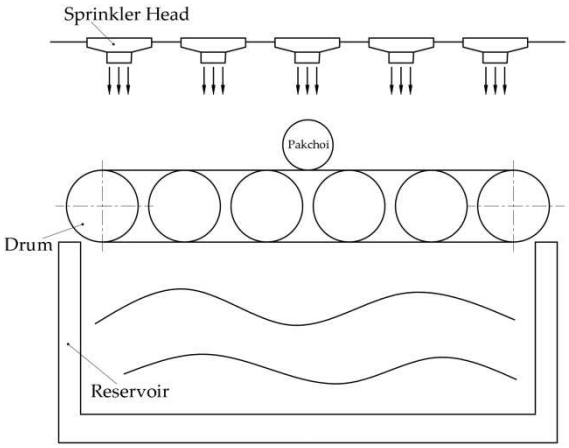


Fig. 3. Schematic of the washing mechanism.

The drum is a critical component of the washing mechanism, and its structural strength must therefore be verified. The parameters of the selected drum are: belt speed v=0.35 m/s, drum length l=300 mm, diameter D=50 mm, wall thickness t=1.2 mm, and the material is Q235 steel plate. According to the fourth strength theory, the allowable contact stress, σh, of the drum is calculated using the following formula:

$$\begin{cases} \sigma = \dfrac{M}{W} \\ \tau = \dfrac{T}{2W_T} \\ \sigma_h = \sqrt{\sigma^2 + 3\tau^2} \end{cases} \quad (2)$$

where σh is the allowable contact stress, MPa; σ is the bending stress, MPa; τ is the shear stress, MPa; M is the bending moment, N·mm; T is the torque, N·mm; W is the section modulus in bending, mm^3; and WT is the section modulus in torsion, mm^3. The strength of the drum body meets the design requirement and is suitable for use.

3.2. Quantitative Packaging Module

This section describes the mechanical design of the quantitative packaging module, which includes three core sub-units: a 90° pakchoi-turning mechanism, an air-drying mechanism, and a tying-packaging mechanism.

3.2.1. 90° Pakchoi -Turning Mechanism

This mechanism mainly consists of a worm-and-wheel transmission, a pakchoi-holding box, and a turning pusher. The worm-and-wheel transmission drives the holding box to rotate 90°, changing the pakchoi from a horizontal to a vertical orientation. The pusher then moves linearly to transfer the pakchoi accurately to the next station. In this way, orientation change and process transfer are coordinated precisely. A schematic of the mechanism is shown in Fig. 4.

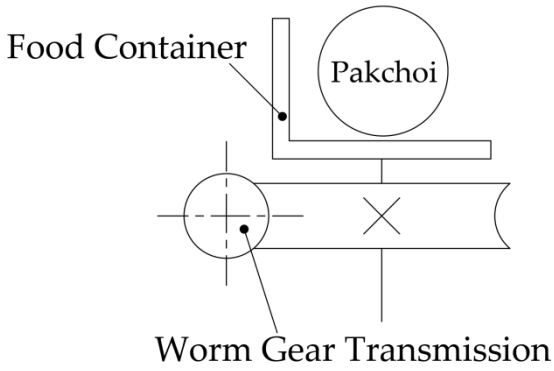


Fig. 4. Schematic of the 90° pakchoi-turning mechanism.

3.2.2. Air-Drying Mechanism

This mechanism is installed directly above the 90° turning unit to ensure a smooth transition between processes. It consists mainly of a centrifugal fan and outlet nozzles. Airflow is guided by a specially designed flow-straightening structure to form a uniform air curtain that rapidly removes surface moisture from the leaves. By adjusting the speed of the drive motor, the air volume and velocity can be controlled flexibly (Dag et al., 2023), thereby ensuring the pakchoi reaches the required dryness before tying and packaging.

3.2.3. Tying-Packaging Mechanism

This unit consists mainly of a rotating ring-wheel, a tape dispenser, a synchronous-belt transmission, and a pneumatic cutter. During operation, the motor rotates the ring-wheel, which causes the tape reel to orbit the central pakchoi bundle, completing the wrapping cycle (ZHANG Wenhan et al., 2023). The inner diameter of the ring-wheel is 250 mm, allowing it to adapt to bundles of different sizes. After wrapping, a single-acting cylinder-driven cutter quickly cuts the tape (Zhang Cong & Chu Hairong, 2002). This design avoids the physical damage that could occur if the pakchoi itself were rotated, and it achieves reliable, efficient automated tying while simplifying the mechanical structure. A schematic of the mechanism is shown in Fig. 5.

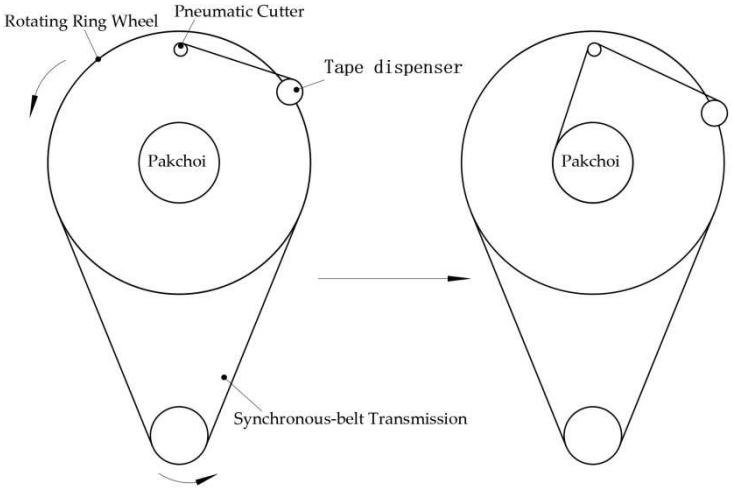


Fig. 5. Schematic of the tying-packaging mechanism.

For a bolt group under a total load $F\Sigma=45$ N acting at an angle $\alpha=50°$ to the vertical (Liang Liansheng & Qiu Xiangwen, 2001), the shear stress on each bolt can be expressed as follows:

$$\begin{cases} F_0 = \dfrac{1}{Z}\left(\dfrac{K_s F_{\Sigma v}}{f} + \dfrac{C_m}{C_b + C_m} F_{\Sigma h}\right) \\ F_2 = F_0 + \dfrac{C_m}{C_b + C_m} F \\ \sigma_{bs\max} = \dfrac{1}{A}\left(ZF_0 - \dfrac{C_m}{C_b + C_m} F_{\Sigma h}\right) + \dfrac{M}{W} \end{cases} \quad (3)$$

where F_0 is the preload per bolt, N; Z is the number of bolts; Ks is the slip factor; $F\Sigma v$ is the lateral force, N; f is the friction coefficient of the interface; $F\Sigma h$ is the axial force, N; Cb/(Cb + Cm) is the relative stiffness of the bolt; F is the working load per bolt, N; F_2 is the total tensile force per bolt, N; σbsmax is the maximum bearing stress, MPa; A is the interface area, mm²; W is the section modulus in bending, mm³; and M is the bending moment, N·mm. The calculation confirms that the lower region of the joint is not crushed and that no gap forms at the least-compressed point on the upper interface.

3.3. Conveying mechanism

The conveying mechanism consists of roller-conveyor units, belt-conveyor units, and chain-and-sprocket drives. Chain transmission synchronizes the modules, with the belt speed set at 0.65 m/s and the roller linear speed at 0.70 m/s, ensuring smooth material flow between successive stages.

3.4. Dimension design

The overall and key functional dimensions of the machine are designed to ensure smooth, efficient, and ergonomic automated processing of pakchoi. The dimensions are based primarily on the typical size range of pakchoi (total length≈200–300 mm, root-end diameter ⩽250 mm), and account for the functional needs of each processing step, the travel of moving mechanisms, and the space required for operation and maintenance. A compact zigzag layout is adopted for the entire machine. The key dimensions are summarized in Table 1.

Table 1. Key design dimensions of the machine.

Critical Dimension	Dimension data(mm)
Machine size (length × width × height)	1517×777×1050
Effective width of the feeding conveyor belt	300
Root-removing rotary blade diameter	150
Cross slide travel for yellow leaf removal	40
Effective length of the spray washing section	550
Effective length of 90° Pakchoi -Turning Mechanism	300
Length of the air outlet on the Air-Drying Mechanism	320
Inner diameter of the lashing ring	250

Based on the dimension design, the overall layout of the key mechanisms—root removal, yellow-leaf removal, washing, 90° turning, and tying-packaging—and a photograph of the physical prototype are shown in Fig.s 6 and 7, respectively.

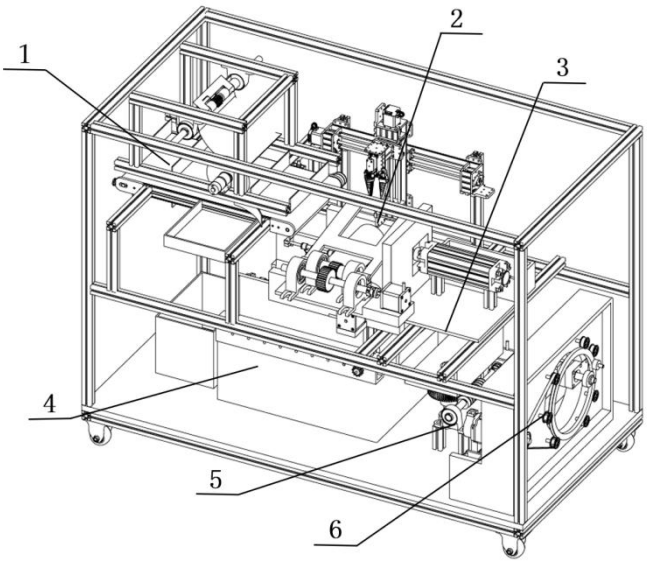


Fig. 6. Schematic of the tying-packaging mechanism. 1. Root-Removal Mechanism. 2. Yellow-Leaf-Removal Mechanism. 3. Air-Drying Mechanism. 4. Washing Mechanism. 5. 90° Pakchoi -Turning Mechanism. 6. Tying-Packaging Mechanism.

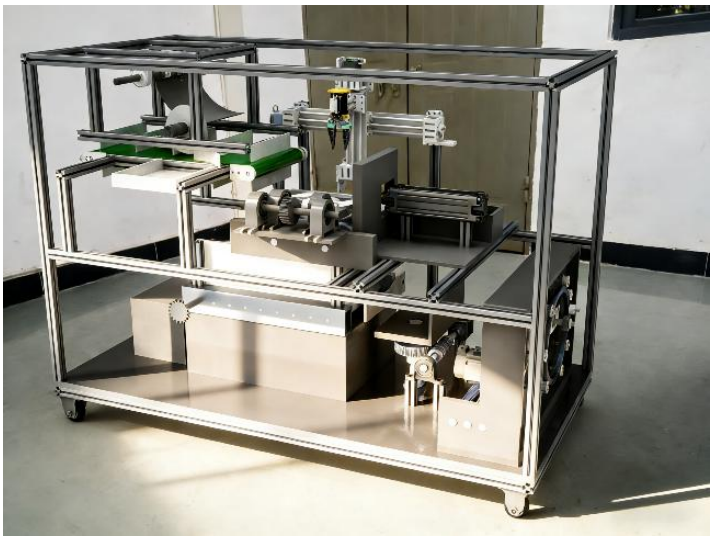


Fig. 7. Schematic of the tying-packaging mechanism.

3.5. Material Selection

In selecting materials, the principles of safety, functionality, durability, and economy are jointly considered (Liu Jun & Ling Zhanjun, 2002). The main frame and housing are constructed primarily from 6061 aluminum-alloy profiles, which provide a favorable combination of light weight, adequate stiffness, and corrosion resistance (XIA Zhanxue et al., 2025). For parts that bear high loads or perform critical transmission roles, such as blade shafts, gears, and guide rails, quenched-and-tempered 45 steel is used to ensure strength, wear resistance, and fatigue performance. All components that contact the pakchoi directly comply with food-hygiene standards: the conveyor belt is made of food-grade PVC; rollers and holding boxes are made of 304 stainless steel, offering corrosion resistance and easy cleaning. The contact surfaces of the flexible gripper are covered with food-grade silicone to avoid leaf damage; its key parameters are listed in Table 2. Auxiliary parts are made of

engineering plastics (e.g., nylon, POM) instead of traditional metals, effectively reducing overall weight while maintaining structural strength and service life.

Table 2. Parameters of Food-Grade Silicone Rubber.

Project	Indicator	Test Method
Tensile strength/MPa	⩾6.5	GB/T 528-2009
Elongation at break/%	⩾350	GB/T 528-2009

3.6. Control System

To ensure the fully automated pakchoi fresh-packaging machine performs all processing steps efficiently, reliably, and in a coordinated way, a modular control system was designed and implemented. The system consists of the following four core modules:

3.6.1. Master Control Module

This module, acting as the control core of the entire electrical system, is based on the STM32F103ZET6 microcontroller. With its high performance and rich peripherals, the microcontroller acquires and processes sensor signals, executes control algorithms, generates motor-driving commands, and coordinates the timing logic among functional modules, thereby ensuring consistent and stable operation of the machine (Li Haolun et al., 2020). To satisfy the real-time requirements of concurrent multi-task execution, a real-time operating system (RTOS) was incorporated for this microcontroller. The RTOS provides essential mechanisms such as task scheduling, message queues, and memory management, enabling priority-based preemption and cooperation among tasks. This improves both system resource efficiency and task responsiveness while effectively avoiding potential resource conflicts during multi-task interaction (Lee et al., 2003). For the specific application of this equipment, the designed task-scheduling scheme and the associated message-queue interaction logic are shown in Fig. 8.

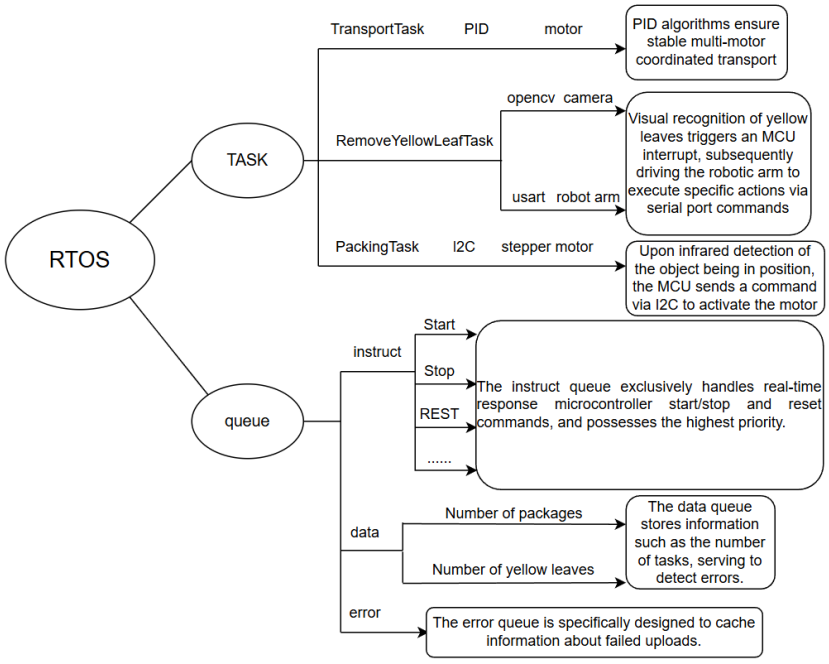


Fig. 8. Task allocation scheme and message queue interaction logic.

3.6.2. Power-Supply Module

As the central power unit of the machine, this module provides stable, safe, and efficient electrical energy to all functional modules (Estévez et al., 2007). It is connected to a 220 V/50 Hz AC mains input, and an LLC-resonant switching topology is used for AC-DC conversion, achieving a typical efficiency above 92% with low loss and wide input-voltage tolerance. Grid fluctuations are effectively suppressed, and system temperature rise is controlled. After rectification, filtering, and regulation, a 24 V DC bus voltage is provided, mainly for driving motors, cylinders, and other high-power actuators (Lee et al., 2016). The module also includes four-stage protection (overcurrent, overvoltage, short-circuit, and overtemperature), which cuts off the output quickly under abnormal conditions to protect the system and the load.

The 24 V DC bus cannot directly supply the control core and other low-voltage circuits. To ensure reliable operation and avoid overheating of the step-down converter, a two-stage power architecture ("DC-DC step-down + LDO regulation") is adopted, which balances conversion efficiency and output ripple. In the first stage, a synchronous-rectification DC-DC buck converter (LM2596S-5.0) reduces the 24 V bus to 5 V with an efficiency over 85%, meeting the power demands of the main board and peripheral sensors. In the second stage, a low-dropout linear regulator (AMS1117-3.3) further stabilises the 5 V supply to 3.3 V for the STM32 core, GPIOs, timers, and other critical peripherals. The output ripple is kept below 50 mV, effectively suppressing high-frequency noise during signal acquisition and processing.

3.6.3. Drive Module

The interface between control commands and mechanical motion, implementing tailored driving schemes according to the dynamic characteristics of different actuators. For the DC motors used in conveying and root-removal units, a PWM speed-control system was built around a BTS7960 H-bridge circuit (Yan et al., 2023). To cope with speed variation and load disturbance in multi-motor coordination, a PID motor-control simulation model was first established in Matlab/Simulink (Fig. 9). PID parameters were tuned, and the control strategy was verified and optimized through simulation; the resulting closed-loop algorithm was then deployed on the actual hardware. The algorithm samples real-time feedback (speed, current, etc.) from each motor and adjusts the PWM duty cycle dynamically through proportional (P), integral (I), and derivative (D) terms (Prajapati & Prasad, 2021), thereby improving the dynamic response, steady-state accuracy, and synchronisation of the multi-motor system. For the pneumatic cylinders in the tying mechanism, a relay-driven solenoid-valve configuration is adopted, providing fast directional switching and precise start-stop control to meet the response (⩽10 ms) and reliability requirements of the tying operation.

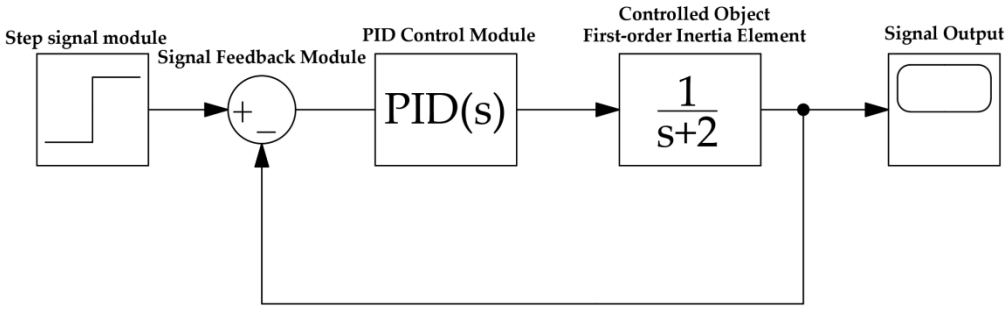


Fig. 9. Block diagram of the PID control simulation model.

3.6.4. Perception and Interaction Module

As the key unit for sensing external states and enabling task coordination, this module integrates infrared photoelectric sensors, limit switches, and a weighing sensor. The vision subsystem is controlled by a dedicated MCU, and its image-processing pipeline follows the classic OpenCV framework, consisting of four main steps:

Ambient-light calibration (Normalization): The current ambient brightness is averaged and used to perform histogram equalization on the image at the algorithm level, reducing the influence of illumination variation on colour fidelity.

HSV colour-space conversion: The acquired RGB image is converted to HSV space (Nazari et al., 2022), where H, S, and V denote hue, saturation, and value, respectively. HSV is preferred over RGB to avoid large data fluctuations caused by changes in the external environment. Processing is performed by an internal algorithm rather than by adjusting camera exposure and gain for the same reason.

Target-colour learning (Feature Learning): When the "Learn" button is pressed, the algorithm extracts the average HSV values (HbaseSbaseVbase) of the pixels in the central region of the image and sets them as the reference for recognition.

Binarization: The system compares each pixel of the live image in real time (Soua et al., 2018). A pixel is classified as the target colour when its HSV values fall within the defined range. For a given pixel P, its hue value H satisfies the following condition:

$$\begin{cases} \left|P_h - H_{base}\right| < Threshold \\ \left(H_{base} - T_h\right) \le H_p \le \left(H_{base} + T_h\right) \\ S_{\min} \le S_p \le S_{\max} \\ V_{\min} \le V_p \le V_{\max} \end{cases} \tag{4}$$

where Hbase is the learned reference hue of the target colour; Th is the hue-tolerance threshold (OpenCV H ranges from 0 to 179); Smax and Smin are the upper and lower saturation limits; V max and Vmin are the upper and lower brightness limits.

The judgment logic for each pixel P in the image is as follows(Soleimanizadeh et al., 2015):

Colour-space conversion: Transform RGB to HSV components using:

$$V \leftarrow \max\left(R, G, B\right)$$

$$S \leftarrow \begin{cases} \dfrac{V - \min\left(R, G, B\right)}{V}, & if \quad V \neq 0 \\ 0 \end{cases} \tag{5}$$

Dynamic-range judgment: Let the learned reference hue be Hbase and the adjustable tolerance threshold be ΔH. The decision function f(P) is:

$$f\left(P\right) = \begin{cases} 1 \quad if \left|H_p - H_{base}\right| \le \Delta H \\ 0 \quad otherwise \end{cases} \tag{6}$$

When the connected area A of pixels satisfying F=1 is smaller than a preset limit, the control-chip I/O port is triggered to toggle.

To test the algorithm's robustness under varying illumination and complex backgrounds, a series of experiments was carried out focusing on colour-tolerance thresholds and related key parameters. Different lighting intensities, colour temperatures, and background textures were simulated, and multiple controlled trials were conducted on the parameters. This allowed a quantitative evaluation and comparison of the recognition accuracy and anti-interference ability of the algorithm in diverse environments. Detailed results are given in Tables 3 and 4.

Table 3. Threshold of Color Tolerance.

Experimental group	Threshold parameter	Recognition success rate	False alarm rate	Response delay (ms)	Performance Evaluation
A(Low)	±5	65%	0.5%	45	rigorous
B(Medium)	±15	98.2%	2.1%	30	optimal
C(High)	±40	100%	35.8%	28	loose

Table 4. Comparison of Color Performance Parameters.

Threshold level	Corresponding physical meaning	Recognition sensitivity	False positive rate	missed detection rate
Low threshold (1–3 settings)	Colour assessment is extremely stringent	Low	Extremely low (Background noise causes virtually no interference)	High (Becomes unrecognisable when light levels drop even slightly)
Medium threshold (4–5 settings)	Permit a certain degree of colour deviation	High	Low (Effectively filters similar background colours)	Low (Stable tracking is maintained even when the target is moving)
High threshold (6–10 settings)	Colour assessment is extremely lenient	Stable	Extremely high (Prone to misidentifying background noise)	Extremely low (Targets are rarely lost)

Comparison shows that the optimal operating point of the system lies in the region of Group B (ΔH=15).

The code-implementation section describes the colour-detection range and I/O control, with the core functions written in C++:

```
1   void processColorDetection(cv::M-at&frame, ColorParams
    &p)
2   {
3   cv::Mat hsv, mask;
4   // 1. Spatial Transformation
5   cv::cvtColor(frame, hsv, cv::COLOR_BGR2HSV);
6   // 2. Constructing Dynamic Threshold Intervals (taking into
```

```
    account the cyclic nature of H channels 0-180)
7   cv::Scalar lower(p.h_base-p.h_tol, p.s_min, p.v_min);
8   cv::Scalar upper(p.h_base+p.h_tol, p.s_max, p.v_max);
9   // 3. Binarisation Segmentation
10  cv:: inRange(hsv, lower, upper, mask);
11  // 4. Noise Reduction Processing (median filtering)
12  cv::medianBlur(mask, mask, 5);
13  // 5. Area Feature Extraction and Logical Determination
14  if (cv::countNonZero(mask) > (frame.total()*0.02))
15  {
16  set_io_high(); //Trigger Flip
17  }
18  else
19  {
20  set_io_low();
21  }
22  }
```

The code processes an input 640 × 480 raw image in the following sequence:

(1)Colour remapping: $RGB \rightarrow HSV$

(2)Threshold slicing: A dynamic threshold [Formula] is applied to extract the target colour region.

(3)Morphological refinement: Median filtering removes isolated noise points.

The proportion of non-zero pixels, n, is then computed. If $n > 2\%$ (i.e., the target colour occupies more than 2 % of the image), set_io_high() is called; otherwise, set_io_low() is executed.

4. Structural Simulation and Performance Analysis

This chapter integrates static simulation, fluid dynamics simulation, and prototype performance testing to systematically verify the structural reliability of key components, characterize the flow-field behavior and associated damage mechanisms during washing, and evaluate the overall processing performance of the complete system.

4.1. Static Analysis

To verify the mechanical feasibility and reliability of the combined leaf-removal and root-cutting actuator, static finite-element analyses were performed on its three main load-carrying parts: the rotary cutting blade, the flexible clamping unit, and the guide-rail slider support. All simulations were carried out in SOLIDWORKS Simulation following established engineering practice (Gouasmi et al., 2012). The purpose was to quantify the stress, deformation, and safety margins of these components under simulated working loads, thereby providing evidence on the design's performance, innovation, and reliability.

As the part directly subjected to cutting forces, the blade governs both cutting efficiency and stability. Static simulation results (Fig. 10) show a maximum von Mises stress of 18.0 MPa, located near the mounting-hole edge, where stress concentrates. The corresponding

maximum elastic strain is 8.161×10^{-5}. This stress is only 8.7 % of the material yield strength (207 MPa), confirming that the blade remains in the linear-elastic range during cutting. Under the design load, the total deformation is 0.0125 mm, indicating high stiffness that maintains cutting-path accuracy and avoids quality loss due to deflection. The minimum safety factor (based on yield) is 9.2, meaning the blade can support more than nine times the nominal load without yielding—providing a substantial buffer against transient shocks from irregular root material.

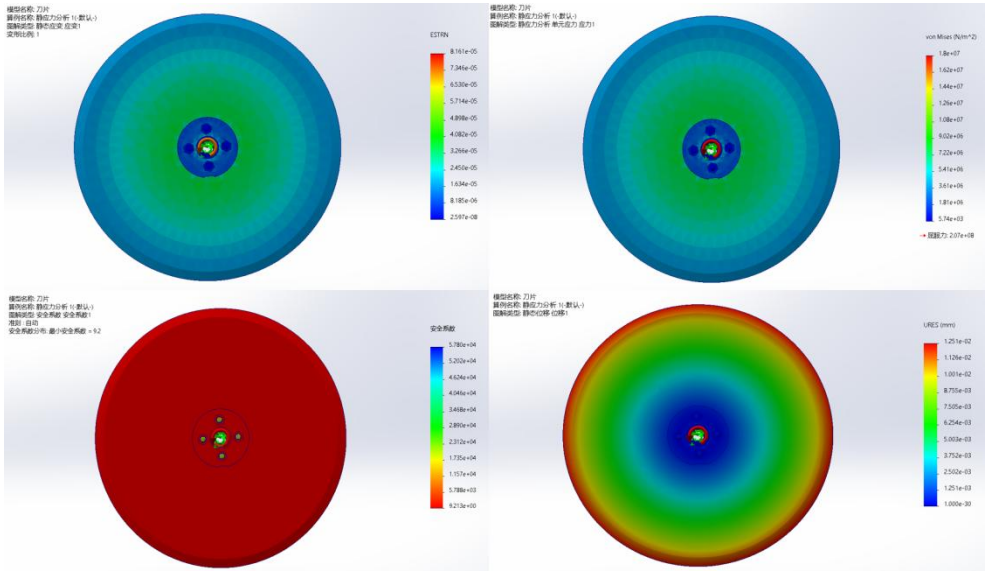


Fig. 10. Static simulation of the root-removal blade.

The flexible gripping unit is designed to deliver adequate clamping force while adapting elastically to root-stems of different diameters, thus enabling non-damaging handling. As seen in Fig. 11, its maximum von Mises stress is 69.39 MPa and its maximum strain 2.00×10^{-4}, both well below the material yield strength (620.4 MPa). A key feature is its 7.00 mm displacement, which lies within the intended elastic range and provides the necessary compliance for adaptive gripping. The unit exhibits a minimum safety factor of 8.9, confirming that sufficient strength is retained even under this functional deformation, thereby avoiding plastic failure.

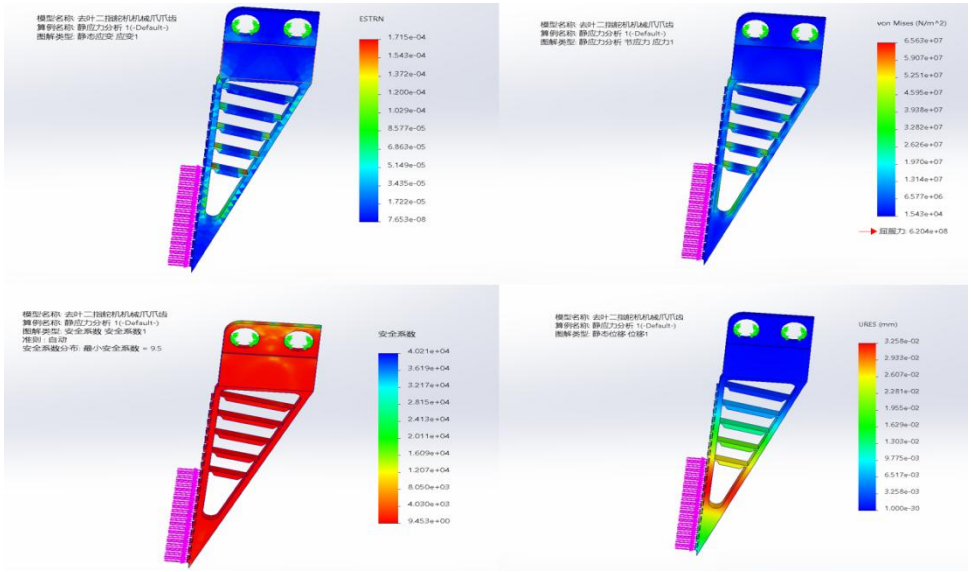


Fig. 11. Static simulation of the flexible gripping unit.

The support base acts as the rigid foundation of the gripping assembly, transmitting the clamping force to the guide rail while ensuring motion accuracy. The simulation (Fig. 12) shows a maximum von Mises stress of 65.63 MPa and a maximum strain of 1.715×10^{-4}, both far below the yield strength of the material (620.4 MPa). Displacement is limited to 0.0326 mm, a micron-level deformation that preserves positioning precision and repeatability during high-speed reciprocation. The safety-factor distribution gives a minimum value of 9.45, with most of the structure exhibiting factors between 10^3 and 10^4, demonstrating the high robustness of this load-bearing component. The static simulation results for these key components are summarized in Table 5.

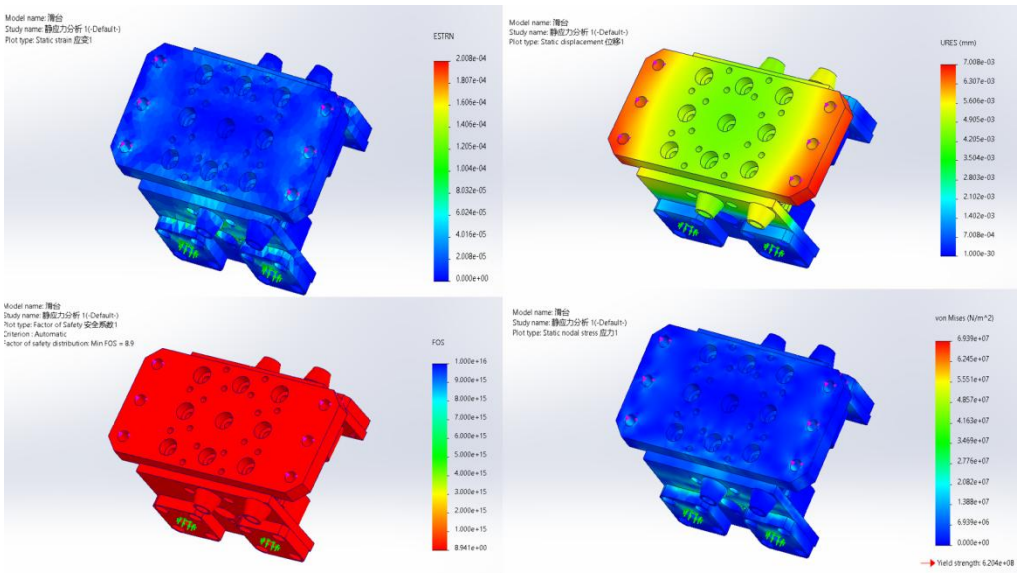


Fig. 12. Static simulation of the guide-rail slider support.

The static simulation results for these key components are summarized in Table 5.

Table 5. Static performance of key components.

Component	Maximum stress (MPa)	Material yield strength (MPa)	Stress utilisation rate(%)	Maximum displacement (mm)	Minimum safety factor
Root-Removal Blade	18.0	207	8.7%	0.0125	9.2
Flexible Gripping Unit	69.39	620.4	11.2%	7.00	8.9
Guide-Rail Slider Support	65.93	620.4	10.6%	0.0326	9.45

The main strength of the design is the system-level co-optimization of function and performance, which delivers high overall reliability while satisfying distinct performance goals. For the cutting blade and the support base, which demand high stiffness, deformation is restricted to the micron scale ($\leqslant$0.033 mm), ensuring motion and cutting accuracy. In contrast, the flexible clamping unit is allowed a millimeter-scale functional displacement (7.0 mm) to achieve nondestructive gripping. Importantly, every component meets its functional requirement with a minimum safety factor of at least 8—well above the

conventional design range (typically 2–4)—thereby establishing a solid basis for system reliability (Sigova & Doronin, 2007). This reflects a graded safety-domain approach and a quantified balance in the rigid-flexible coupled system, while also pointing toward potential weight-reduction paths.

The reliability of the simulation results is supported by a rigorous workflow and cross-validation. Parameters were assigned based on biomechanical test data that included dynamic factors, and material selection was tightly coupled to functional needs. Mesh-independence was verified (maximum stress variation < 2.5 %), ensuring numerical convergence; the resulting data obey mechanical principles and show good consistency (Meng et al., 2025). As a result, every critical component achieves a safety factor not lower than 8, providing a wide engineering safety buffer that can absorb typical uncertainties in loading, material properties, and manufacturing. This thoroughly confirms the mechanical robustness and effectiveness of the actuator design, establishing a solid foundation for low-damage, high-precision operation.

4.2. Fluid Mechanics Simulation

To accurately assess and optimise the performance of the washing unit, computational fluid dynamics (CFD) was used to simulate the flow field during spray cleaning. The purpose was to examine the design from a fluid-mechanical standpoint and, through a systematic parameter study (Lintermann, 2021), to identify the operating conditions that provide effective cleaning while keeping physical damage to the leaves as low as possible.

A closed computational domain that included an array of nozzles, a rotating drum, a simplified pakchoi model, and a circulating water tank was constructed from the 3D geometry of the equipment (Wan Baoai, 2013). To represent the influence of the pakchoi body more realistically, the pakchoi region was treated as an isotropic porous medium with appropriate porosity and surface roughness. The domain was meshed with polyhedral cells, and boundary-layer refinement was applied in the nozzle-jet core and near the pakchoi surfaces, resulting in about 5.2×10^6 elements. Grid-independence was examined by comparing coarse (2.5×10^6), medium (5.2×10^6), and fine (8.0×10^6) mesh schemes (Fig. 13).

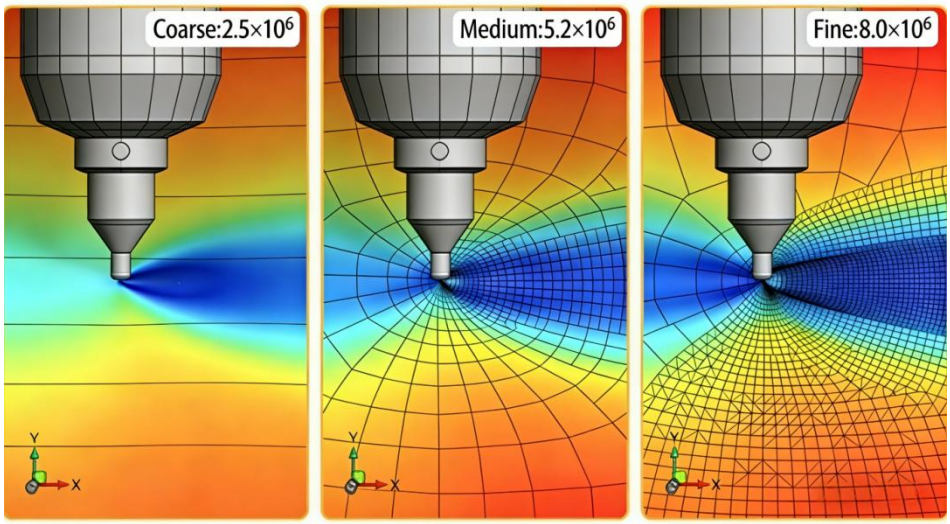


Fig. 13. Mesh of the core region of the nozzle jet.

The average shear stress on the pakchoi surface was chosen as the main monitoring quantity. Results from the three grids differed by less than 2.1 %, indicating that the medium-density

mesh already gives a grid-independent solution (Lomax et al., 2001). The physical model used a pressure-based transient solver together with the Realizable k-ε turbulence model and the VOF multiphase model to resolve the gas-liquid interface. Boundary conditions were set as follows: the nozzle inlet was a pressure inlet with pressure varied between 0.15 and 0.30 MPa; the outlet was ambient pressure; all solid walls were no-slip; the drum wall was given a linear velocity of 0.70 m/s, matching the conveyor belt. The time step in the transient simulation was adjusted adaptively according to the Courant number, maintaining a balance between computational speed and numerical stability.

Flow-field results (Fig. 14) show streamlines and static-pressure contours on a symmetry plane of the domain. The simulation reveals that a high-speed jet (core velocity ≈ 18 m/s) exiting the nozzle strikes the vegetable surface, producing strong local shear. Rotation of the drum generates intricate secondary flows and vortices within the leaf gaps, which noticeably improve water penetration and scouring of leaf backsides and folded regions. To quantify the potential mechanical injury during washing, the peak dynamic pressure on every surface element over a full cleaning cycle was recorded.

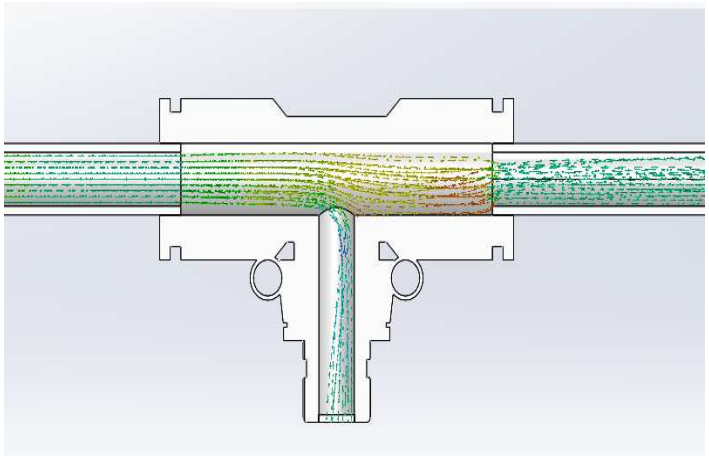


Fig. 14. CFD Flow Field Analysis of the Nozzle.

Based on CFD data from 10000 surface cells of the vegetable body (three-dimensional distribution shown in Fig. 15), the dynamic pressure peaks follow a distinct positive-skewed distribution. Statistics indicate that more than 99.5 % of the sampled cells experienced peak pressures below 48.2 kPa, and 99.96 % remained under 50 kPa. These values lie well below the structural-damage threshold of pakchoi leaf-tissue cell walls reported in biomechanical studies (typically >200 kPa). The comparison quantitatively confirms that the spray-cleaning system designed here supplies enough fluid shear for effective cleaning while keeping the mechanical load safely within the tolerable range of the vegetable tissue, thereby providing a physical basis for the low-damage performance of the process.

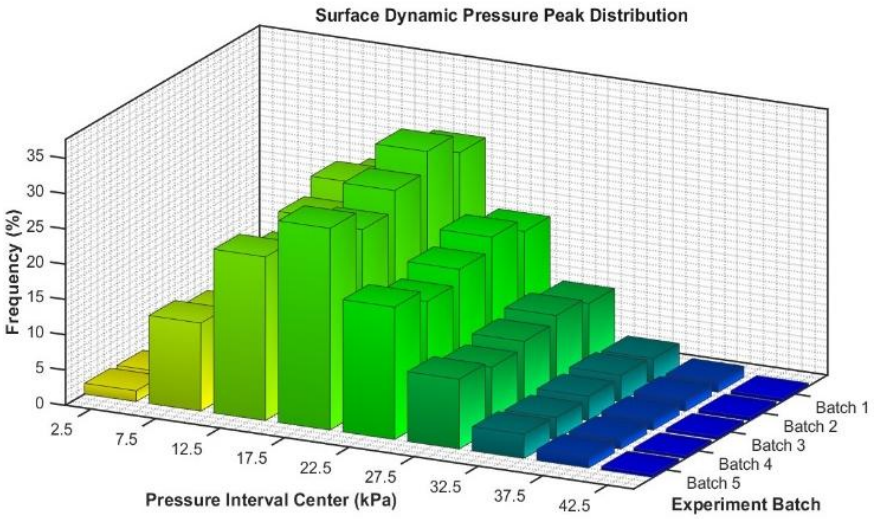


Fig. 15. Peak dynamic pressure on the pakchoi surface.

Nozzle pressure is a key adjustable parameter affecting both cleaning performance and operating cost. To identify its optimum, a parametric CFD study combined with experimental validation was carried out (DONG Yongcan et al., 2025). With the conveyor speed fixed at 0.70 m/s, four pressure levels (0.15, 0.20, 0.25, and 0.30 MPa) were tested for cleaning efficiency and water use per unit output. As shown in Fig. 16, cleaning efficiency approached a saturation plateau with rising pressure, while water consumption increased almost linearly. Specifically, raising the pressure from 0.25 MPa to 0.30 MPa improved cleaning by only 0.6 percentage points (from 97.2 % to 97.8 %), but increased water use from 2.9 L/kg to 3.5 L/kg—a jump of over 20 %. Following the principle of diminishing marginal returns, 0.25 MPa was selected as the optimum operating pressure. At this pressure, cleaning efficiency exceeds 97 %, satisfying commercial requirements, and a good balance between cleaning effectiveness and water consumption is achieved.

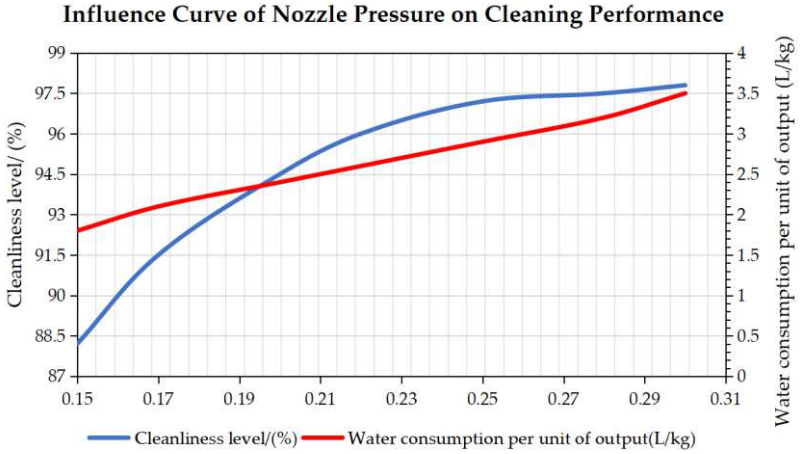


Fig. 16. Nozzle pressure versus cleaning performance.

Based on the principle of diminishing marginal returns, 0.25 MPa was identified as the most economical operating pressure. At this level, cleaning efficiency (97.2 %) satisfies commercial requirements (>97 %) and lies near the inflection point of the performance-saturation curve. Increasing pressure to 0.30 MPa would raise cleanliness by only 0.6 percentage points while increasing water consumption by 20.7 %, significantly lowering the energy efficiency of the

system (Faff et al., 2013). This trade-off analysis yields a clear, quantified operating point, providing a scientifically grounded basis for running the equipment.

By combining CFD simulation with experiment, this analysis explains the flow mechanisms behind the unit's efficient cleaning and low-damage behaviour and, through rigorous parameter optimization, supplies quantified guidance for practical operation. As a result, the washing system design moves beyond traditional trial-and-error approaches and is founded on a basis of predictable simulation supported by experimental verification.

4.3. Performance Tests

After assembly and commissioning, the prototype was tested for functionality and performance. The main results are as follows:

(1)Throughput: The machine operated stably at ⩾50 kg/h, well above the manual rate of 20–30 kg/h per worker. Full automation from root removal to packaging eliminated transition delays and manual handling.

(2)Product quality: Root removal reached 100 %, yellow-leaf removal exceeded 98 %, and leaf damage was kept below 3 %. The combination of machine vision and flexible actuation gave a damage rate notably lower than that of manual work (typically 5–10 %) or of non-specialised leaf-vegetable equipment (Mepba et al., 2007).

(3)Operational stability: No failure occurred during 8 h of continuous running. All mechanisms worked together reliably, showing better long-term stability than manual operation or many general-purpose machines.

5. Conclusions

This study developed a fully automated integrated processing machine for pakchoi by adopting an innovative zigzag layout and modular design based on the material and processing characteristics of leafy pakchois. Finite element simulations confirmed that the key functional mechanisms satisfy the required strength and stiffness criteria with sufficient safety margins. Prototype tests further verified that the equipment meets the expected standards in processing efficiency, product quality, and operational stability. The system effectively addresses the lack of integrated automated processing equipment for leafy pakchois, with the main innovations reflected in the following aspects:

(1)Integration of eight consecutive processing steps—from feeding to packaging—enables continuous one-stop production, substantially reducing manual intervention;

(2)A combination of machine vision and flexible gripping allows accurate identification and nondestructive removal of yellow leaves, preserving the commercial quality of the final product;

(3)The zigzag spatial arrangement optimizes the layout of functional modules, improving floor-space utilization;

(4)An intelligent control system with a human-machine interface supports flexible adjustment of operating parameters according to different production scenarios.

The machine is suitable for fresh-food logistics companies, central kitchens, and supermarket back-end processing centers, and is expected to promote the automation and standardization of leafy-pakchoi processing with promising application prospects.

Author Contributions: "Conceptualization, Lin Zongde and Yu Ping; methodology, Lin Zongde and Lin Peng; software, Deng Jiakun and Xue Hongwei; validation, Lin Zongde, Yu

Ping and Lai Shengwei; formal analysis, Lin Peng and Deng Jiakun; investigation, Xue Hongwei and Huang Senhui; resources, Lin Zongde and Lai Shengwei; data curation, Deng Jiakun and Huang Senhui; writing—original draft preparation, Lin Zongde and Yu Ping; writing—review and editing, Lin Peng and Xue Hongwei; visualization, Lai Shengwei and Huang Senhui; supervision, Lin Zongde; project administration, Yu Ping; funding acquisition, Lin Zongde. All authors have read and agreed to the published version of the manuscript."

Data Availability Statement: The datasets generated and/or analysed during the current study are available from the corresponding author on reasonable request.

Acknowledgments: Min Nan University of Technology Opto-Mechatronics Innovation Team (23XTD111) Fujian Provincial Key Laboratory of Industrial Robot Measurement, Control and Mould Rapid Manufacturing (Min Jiao Ke [2017] No. 8)

Funding： This work was financially supported by the Opto-Mechatronics Innovation Team (No. 23XTD111) of Minnan University of Science and Technology, and the Fujian Provincial Key Laboratory of Industrial Robot Measurement, Control and Mould Rapid Manufacturing (Grant No. Min Jiao Ke [2017] No. 8).

Conflicts of Interest: Declare conflicts of interest or state “The authors declare no conflicts of interest.” Authors must identify and declare any personal circumstances or interests that may be perceived as inappropriately influencing the representation or interpretation of reported research results. Any role of the funders in the design of the study, in the collection, analyses, or interpretation of data, in the writing of the manuscript, or in the decision to publish the results must be declared in this section. If there is no role, please state “The funders had no role in the design of the study; in the collection, analyses, or interpretation of data; in the writing of the manuscript; or in the decision to publish the results”.

References

1. Accelerating the Pilot Verification and Maturation Application of Innovative Agricultural Machinery Products. (2025). *Yunnan Agriculture*, *39*(11), 9–10.
2. Da Silva, V. H., Murphy, F., Amigo, J. M., Stedmon, C., & Strand, J. (2020). Classification and quantification of microplastics (<100 μm) using a focal plane array–fourier transform infrared imaging system and machine learning. *Analytical Chemistry*, *92*(20), 13724–13733.0c01324
3. Dag, D., Farmanfarmaee, A., Kong, F., Jung, J., McGorrin, R. J., & Zhao, Y. (2023). Feasibility of simultaneous drying and blanching inshell hazelnuts (corylus avellana L.) using hot air–assisted radio frequency (HARF) heating. *Food and Bioprocess Technology*, *16*(2), 404–419.1007/s11947-022-02946-6
4. DONG Tingjian, ZHANG Ji, WANG Danfeng, & WU Mengli. (2023). Design and Research of Elastic Finger Joint Structure for High-Simulation Anthropomorphic Robotic Hand. *Machinery Design & Manufacture*, (9), 253–257.006
5. DONG Yongcan, YUAN Xingfei, LI Shu, & AKRAM Samy. (2025). Structural Design and Deployment Analysis of a Novel Rib-Patterned Deployable Antenna Structure. *Journal of South China University of Technology(Natural Science Edition)*, *49*(11), 63–69.008

6. EFSA Panel on Biological Hazards (BIOHAZ), Koutsoumanis, K., Ordóñez, A. A., Bolton, D., Bover-Cid, S., Chemaly, M., De Cesare, A., Herman, L., Hilbert, F., Lindqvist, R., Nauta, M., Nonno, R., Peixe, L., Ru, G., Simmons, M., Skandamis, P., Suffredini, E., Banach, J., Ottoson, J., … Allende, A. (2023). Microbiological hazards associated with the use of water in the post-harvest handling and processing operations of fresh and frozen fruits, vegetables and herbs (ffFVHs). Part 1 (outbreak data analysis, literature review and stakeholder questionnaire). *EFSA Journal*, *21*(11).8332
7. Estévez, E., Marcos, M., & Orive, D. (2007). Automatic generation of PLC automation projects from component-based models. *International Journal of Advanced Manufacturing Technology*, *35*(5–6), 527–540.1007/s00170-007-1127-4
8. Faff, R., Ho, Y.-K., Lin, W., & Yap, C.-M. (2013). Diminishing marginal returns from R&D investment: Evidence from manufacturing firms. *Applied Economics*, *45*(5), 611–622.608644
9. Gouasmi, M., Ouali, M., Fernini, B., & Meghatria, M. (2012). Kinematic modelling and simulation of a 2-R robot using SolidWorks and verification by MATLAB/simulink. *International Journal of Advanced Robotic Systems*, *9*(6), 245.5772/50203
10. Hao, G., & Hand, R. B. (2016). Design and static testing of a compact distributed-compliance gripper based on flexure motion. *Archives of Civil and Mechanical Engineering*, *16*(4), 708–716.011
11. HE Xiaodong, ZHU Dequan, ZHU Jianjun, LIAO Juan, ZHANG Shun, & LI Jingfa. (2020). Design and experiment on washer with two-speed hair brush rollers for fruits. *Acta Agriculturae Zhejiangensis*, *32*(9), 1702–1710.
12. Henny, R. L., & Gobilik, J. (n.d.). *Overview on leafy (Pak Choy) vegetable industry and vertical soilless culture application for Pak Choy production in Malaysia*.
13. Lee, J., Mooney, V. J., Daleby, A., Ingström, K., Klevin, T., & Lindh, L. (2003). A comparison of the RTU hardware RTOS with a hardware/software RTOS. *Proceedings of the 2003 Conference on Asia South Pacific Design Automation - ASPDAC*, 683.1119925
14. Lee, J.-B., Kim, J.-K., Baek, J.-I., Kim, J.-H., & Moon, G.-W. (2016). Resonant capacitor on/off control of half-bridge LLC converter for high-efficiency server power supply. *IEEE Transactions on Industrial Electronics*, *63*(9), 5410–5415.2558481
15. Li Haolun, Hu Jianing, Zhan Yu, & Li Dongming. (2020). Design of Control System Based on STM32 Multi-function Remote Agriculture Vehicle. *Journal of Agricultural Mechanization Research*, *42*(2), 261–264, 268.050
16. Liang Liansheng & Qiu Xiangwen. (2001). An Agricultural Trial Type Fully Automatic Packaging Machine for Leafy Vegetables. *Fujian Agricultural Machinery*, (3), 21.
17. Lintermann, A. (2021). Computational meshing for CFD simulations. In K. Inthavong, N. Singh, E. Wong, & J. Tu (Eds), *Clinical and biomedical engineering in the human nose* (pp. 85–115). Springer Singapore.1007/978-981-15-6716-2_6
18. Liu Jun & Ling Zhanjun. (2002). The Material Choice of Agricuture Machinery Parts. *Journal of Agricultural Mechanization Research*, (4), 92–93.035
19. Liu Shihao, Zhao Hongyang, Wang Jianbo, & LI Zainian. (2017). A Vegetable Cutting Machine Based on CrankLink Mechanism. *Southern Agricultural Machinery*, *48*(13), 32.
20. Lomax, H., Pulliam, T. H., & Zingg, D. W. (2001). *Fundamentals of computational fluid dynamics*. Springer Berlin Heidelberg.1007/978-3-662-04654-8
21. Luan, C., Zhang, M., Fan, K., & Devahastin, S. (2021). Effective pretreatment technologies for fresh foods aimed for use in central kitchen processing. *Journal of the Science of Food and Agriculture*, *101*(2), 347–363.10602
22. Martinez, R. V., Glavan, A. C., Keplinger, C., Oyetibo, A. I., & Whitesides, G. M. (2014). Soft actuators and robots that are resistant to mechanical damage. *Advanced Functional Materials*, *24*(20), 3003–3010.201303676

23. Meng, L., Wang, R., Peng, W., Shao, J., & Liu, J. (2025). Dynamic and static simulation of electromechanical equipment considering the influence of service environment. *IET Conference Proceedings*, *2024*(13), 2377–2384.3373
24. Mepba, H. D., Eboh, L., & Banigo, D. E. B. (2007). Effects of processing treatments on the nutritive composition and consumer acceptance of some nigerian edible leafy vegetables. *African Journal of Food, Agriculture, Nutrition and Development*, *7*(1).php/ajfand/article/view/136145
25. Nazari, K., Ebadi, M. J., & Berahmand, K. (2022). Diagnosis of alternaria disease and leafminer pest on tomato leaves using image processing techniques. *Journal of the Science of Food and Agriculture*, *102*(15), 6907–6920.12052
26. Palamarchuk, I., Palamarchuk, V., Gudzenko, M., Sarana, V., & Mukoid, R. (2021). Hydrolysis of vegetable raw pectin-containing materials under vibration and centrifugal mixing of liquid environment. In V. Ivanov, I. Pavlenko, O. Liaposhchenko, J. Machado, & M. Edl (Eds), *Advances in design, simulation and manufacturing IV* (pp. 277–286). Springer International Publishing.1007/978-3-030-77823-1_28
27. Prajapati, A. K., & Prasad, R. (2021). A novel order reduction method for linear dynamic systems and its application for designing of PID and lead/lag compensators. *Transactions of the Institute of Measurement and Control*, *43*(5), 1226–1238.1177/0142331220974173
28. Shi, L., Zheng, W., Lei, T., Liu, X., & Hui, M. (2021). The effect of different soil amendments on soil properties and on the morphological and physiological characteristics of chinese cabbage. *Journal of Soil Science and Plant Nutrition*, *21*(2), 1500–1510.1007/s42729-021-00456-6
29. Sigova, E. M., & Doronin, S. V. (2007). Computed estimate of safety factors for shell elements of production equipment. *Chemical and Petroleum Engineering*, *43*(11–12), 647–652.1007/s10556-007-0115-8
30. Soleimanizadeh, S., Mohamad, D., Saba, T., & Rehman, A. (2015). Recognition of partially occluded objects based on the three different color spaces (RGB, YCbCr, HSV). *3D Research*, *6*(3), 22.1007/s13319-015-0052-9
31. Soua, M., Kachouri, R., & Akil, M. (2018). GPU parallel implementation of the new hybrid binarization based on kmeans method (HBK). *Journal of Real-Time Image Processing*, *14*(2), 363–377.1007/s11554-014-0458-2
32. Wan Baoai. (2013). The application of simulation technology in the design of agricultural. *Hunnan Agricultural Machinery*, *40*(1), 51–52.
33. XIA Zhanxue, ZHANG Xiaofeng, FU He, ZHANG Minjie, & CHAO Yuelin. (2025). Application Status and Development of Steel for Agricultural Machinery in China. *Tractor & Farm Transporter*, *52*(4), 5–8, 28.
34. Yan, B., Huang, H., & Wang, H. (2023). PSC-PWM modulated MPC for cascaded H-bridge power supplies. *Journal of Power Electronics*, *23*(5), 746–757.1007/s43236-022-00579-8
35. Yang, P., Zang, J., Huang, B., & Zhao, J. (2025). Electromagnetically adhering and self-inductive sensing claw for continuum climbing robots: Design, control, and applications. *Advanced Intelligent Systems*, *7*(7), 2400800.202400800
36. Zhang Cong & Chu Hairong. (2002). The Modular Design and the Research of the Control Systemfor the Automatic Form-Fill-Seal Machine. *Packaging and Food Machinery*, (5), 1–3, 12.
37. Zhang Minggui, Qu Jun, & Liu Huocheng. (2024). Application of machine vision-based 3D reconstruction technology in vegetables: A review. *Jiangsu Agricultural Sciences*, *52*(9), 27–35.004
38. ZHANG Wenhan, WANG Guanping, & HE Chengzhu. (2023). Causes and improvement of empty packaging of three-servopillow vegetable packaging machine. *Forestry Machinery & Woodworking Equipment*, *51*(10), 44–50.008
39. Zhao Yongcheng & Luo Jinhai. (2025). Innovative Design and Analysis of a New-Type Vegetable Washing Machine. *China Agricultural Machinery Equipment*, (7), 54–57.